

Straight cracks in dynamic brittle fracture

O. Pla¹, F. Guinea¹, E. Louis², S.V. Ghaisas³, and L. M. Sander⁴

¹ *Instituto de Ciencia de Materiales, Consejo Superior de Investigaciones Científicas, Cantoblanco, E-28049 Madrid, Spain.*

² *Departamento de Física Aplicada, Universidad de Alicante, Apartado 99, E-03080 Alicante, Spain.*

³ *Department of Electronics Science, University of Pune, Pune 411007, India*

⁴ *Physics Department, The University of Michigan, Ann Arbor MI 48105-1120. USA*

(June 13, 2021)

We study the dynamics of cracks in brittle materials when the velocity of the crack is comparable to the sound velocity by means of lattice simulations. Inertial and damped dynamics are analyzed. It is shown that dissipation strongly influences the shape of the crack. While inertial cracks are highly unstable, dissipation can stabilize straight cracks. Our results can help to explain recent experiments on PMMA.

I. INTRODUCTION.

The dynamics of cracks in brittle materials such as glasses has recently attracted a great deal of interest. While an extensive body of work exists on the properties of quasistatic cracks, crack propagation when the crack grows at velocities comparable to the sound velocity is still poorly understood (see¹). Particular attention has been devoted to the study of crack tip instabilities such as crack branching and oscillation²⁻⁶. Typically, the crack tip reaches a critical velocity of the order of the Rayleigh speed in the material; faster cracks branch or oscillate. Interesting patterns were also observed under an applied thermal gradient⁷.

In the following, we analyze crack tip instabilities in brittle materials. In these systems, the stress distribution around the crack is assumed to be well described by the continuum theory of elasticity⁸. We assume that the instabilities observed in the experiments cited above are determined by these stresses.

The stress distribution near the tip of a moving crack was analytically calculated by Yoffe⁹. The calculation shows a bifurcation at a critical velocity $c_Y \approx 0.6c_R$ where c_R is the Rayleigh velocity. Beyond this velocity, the stress component tangent to the crack tip ($\sigma_{\theta\theta}(r, \theta)$, assuming that the tip has radius of curvature, r) has a maximum at a finite angle θ with the crack direction. This result can be interpreted as a tendency for the crack tip to deviate from the straight direction.

This criterion is the simplest which predicts an instability of an inertial crack. Alternative criteria can be obtained by slightly perturbing the crack shape, and looking for the growth of the perturbation. In¹⁰, a wavy perturbation is added to a straight, quasistatic crack, and the induced modifications of the stresses at the tip are calculated. An instability is identified when the shear stresses are enough to deviate the crack from its initial directions. In this quasistatic case, a finite external shear is required to induce the instability. This analysis is extended to dynamical cracks in¹¹, where it is shown that above a certain velocity an infinitesimal shear distortion is amplified. The critical velocity depends on material

parameters which describe the forces at the crack tip. Quasistatic cracks in PMMA under different stress distributions follow trajectories well described in terms of the stress intensity factor near the crack tip¹².

We now concentrate on cracks in PMMA, which is a glassy polymer. The microscopic aspects of the fracture process are not understood. It is possible to define a characteristic length in terms of the tensile strength, f_t , the crack surface energy, G_F , and the Young's modulus of the material. The standard definition for thick plates and planar deformations is¹³ $l_{ch} = EG_F / ((1 - \nu^2)f_t^2)$. This length, derived from macroscopic parameters, gives an estimate of the scale at which continuum elasticity may cease to be valid. Using the parameters in Table I, we find: $l_{ch} \approx 60.2$ microns¹³. Typical structures at the crack tip, such as its radius of curvature, have dimensions comparable to this length. Thus, a comprehensive model of the growing crack should, at least, take into account physical phenomena beyond this scale. Elastic waves of wavelengths of micrometers have frequencies in the gigahertz range.

c_e (cal g ⁻¹ K ⁻¹)	0.28
κ (cal cm ⁻¹ s ⁻¹ K ⁻¹)	4.7×10^{-3}
ρ (g cm ⁻³)	1.2
$1/(\kappa\rho c_e)$	6.3×10^3
E (GPa)	2.9
ν (Poisson ratio)	0.401
G_F (N m ⁻¹)	290
f_t (MPa)	130
c_R (m s ⁻¹)	989

TABLE I. Experimental values for some constants of PMMA relevant to the present work. The meaning of the symbols is: c_e , specific heat, κ , thermal conductivity, ρ , density, E , Young's modulus, G_F , crack surface energy, f_t , tensile strength, and c_R , Rayleigh velocity.

In the following we will analyze cracks in PMMA by means of an approximate model in which details at the atomic and molecular scale are neglected. We take it as a coarse-grained approximation to a more microscopic description in order to gain information on the role of effective macroscopic parameters on the shape of the growing crack. The model has already been used in studying the influence of thermal gradients on crack growth¹⁴. As we will discuss, we find that the viscosity (which determines the sound attenuation, for instance) plays a major role in stabilizing straight cracks and controlling their instabilities.

In the following section, we give a brief discussion of the experimental situation. Then, we discuss the model, its general features, and related results available in the literature. We next present our results. The following section discusses possible improvements of the model, and the article ends with a conclusion section. There is an appendix where possible mechanisms which may lead to dissipation in PMMA are explored.

II. EXPERIMENTAL FACTS

The propagation of cracks, under mode I conditions, in PMMA shows different regimes²⁻⁶. Most experiments are done in PMMA sheets under uniaxial stress. An initial straight crack grows with a velocity dependent on the applied stress. Above a certain threshold, the velocity shows oscillations in time, although the crack remains straight. At higher values of the average velocities the crack surface becomes rough due to the formation of microscopic side branches (microbranching transition). At even higher velocities, the crack branches into several paths. The transition from velocity oscillations (and acoustic emission) to microbranching is accompanied by a discontinuity in the average velocity. These transitions take place at velocities which are a fraction of the Rayleigh velocity, $c_R = 989$ m/s. Only a small fraction of the energy dissipated during the growth process is radiated into sound waves⁶. Significant heating effects have been reported¹⁵. When the growing crack is perturbed by means of external sound sources, many features of the previous picture are modified¹⁶. The velocity gap at the microbranching transition is washed out.

The previous picture also seems to hold for cracks in ordinary glass¹⁷. Cracks moving at constant speed seem, however, much more difficult to stabilize in ordinary glass than in PMMA¹⁸.

III. DISSIPATION IN PMMA

Elastic waves are attenuated in real materials, and energy is transferred to degrees of freedom other than those which describe sound waves. This attenuation can be

modeled by adding a viscosity term⁸ to the elastic equations of motion of the form $\eta \nabla^2 \partial_t \mathbf{u}$ where \mathbf{u} is the displacement, and η is a viscosity coefficient. In this long-wavelength limit transverse sound waves acquire an attenuation $\alpha = \eta k^2 / 2\rho c_T$ where ρ is the density and c_T is the transverse sound velocity. Thus there is a wave-vector at which the attenuation of a wave becomes comparable to its wavelength, $\alpha \Lambda = \pi \eta k / \rho c_T \sim 1$. Beyond this scale, sound waves are overdamped, and the analysis reported in⁹ certainly needs to be modified.

The influence of a different form of viscosity on the velocity of straight cracks was considered in¹⁹. It was found that the presence of damping at the edges of a type III crack leads to a steady state velocity which, at high viscosities, is inversely proportional to the damping coefficient.

The term $\eta \nabla^2 \partial_t \mathbf{u}$ is thought to be appropriate at very low frequencies. However, in glassy systems the attenuation is a complicated function of frequency due to the different relaxation processes which contribute²⁰. For example, for PMMA at high frequencies (several GHz), $\alpha \Lambda \sim 0.1$ ^{21,22}, and, thus, $\alpha \propto \omega$. At lower frequencies (2 MHz), the dependence of α on frequency can be fitted by a power law, $\alpha \sim \omega^c$, with $c \sim 1.5 - 1.7$ ²³. It has been argued that some relaxation processes freeze below 165K²⁴. It is likely that, at frequencies < 100 GHz a dependence other than ω^2 may arise. At sufficiently low temperatures, the situation simplifies somewhat, as the main modes which contribute to dissipation are better understood²⁵. A microscopic analysis of dissipation processes at low temperatures, using as input detailed experimental data on the low energy modes in glassy polymers²⁶, is given in the Appendix.

IV. GENERAL FEATURES OF CRACKS IN BRITTLE SOLIDS

A. The Equations of Motion

The equations of motion including viscous terms for an isotropic medium can be written as:

$$\rho \partial_{tt} \mathbf{u} = \mu \nabla^2 \mathbf{u} + (\lambda + \mu) \nabla (\nabla \cdot \mathbf{u}) + \eta \nabla^2 \partial_t \mathbf{u} + (\psi + \eta) \nabla (\nabla \cdot \partial_t \mathbf{u}), \quad (1)$$

where \mathbf{u} is the displacement field, λ and μ the Lamé coefficients and ψ and η the corresponding coefficients in the viscous case.

B. Attenuation of Elastic Waves

The relation between the attenuation coefficient and the frequency can be derived approximating the solutions of the equations of motion by a longitudinal plane wave,

$$\mathbf{u}(\mathbf{r}, t) = \mathbf{u}_0 e^{i[(k+i\alpha)x - \omega t]} \quad (2)$$

where $\mathbf{u}_0 = u_0 \hat{\mathbf{i}}$ is the amplitude of the wave and $\hat{\mathbf{i}}$ the unit vector in the x -direction. The result for the attenuation coefficient is,

$$\alpha = \omega \sqrt{\frac{\rho}{2}} \left[\frac{1}{\sqrt{(\lambda + 2\mu)^2 + (\psi + 2\eta)^2 \omega^2}} - \frac{\lambda + 2\mu}{(\lambda + 2\mu)^2 + (\psi + 2\eta)^2 \omega^2} \right]^{\frac{1}{2}} \quad (3)$$

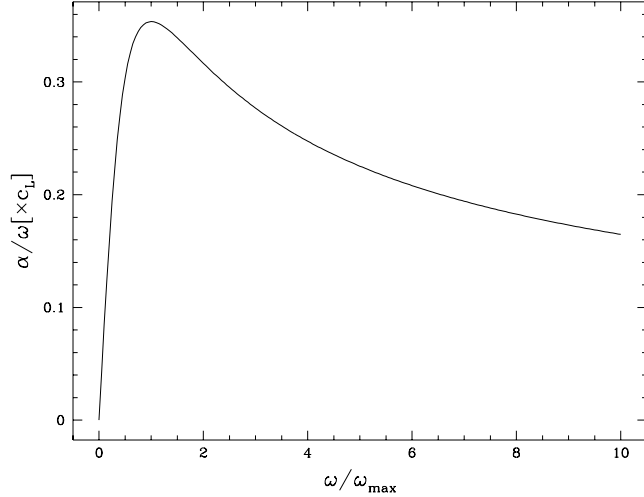


FIG. 1. Attenuation coefficient divided by the frequency as function of the frequency obtained for longitudinal plane waves (see text). The frequency is expressed in units of the frequency at which the maximum occurs (ω_{\max}).

The dispersion relation ($k(\omega)$) is just Eq. 3 changing in the right hand side the minus sign by a plus sign. In Fig. 1 we plot α/ω versus ω/ω_{\max} . This ratio has a maximum at,

$$\omega_{\max} = \sqrt{3} \frac{\lambda + 2\mu}{\psi + 2\eta} \quad (4)$$

and the behavior of the attenuation coefficient in the low and high frequency limits is,

$$\omega \rightarrow 0, \quad \alpha \propto \omega^2 \quad (5a)$$

$$\omega \rightarrow \infty, \quad \alpha \propto \omega^{1/2} \quad (5b)$$

These results show that, roughly, the attenuation coefficient saturates at wavelengths at which the attenuation and the frequency of the wave become comparable. On the other hand, the behavior at low frequencies is consistent with the experimental data and with the results obtained by means of the microscopic analysis described in the Appendix. At high frequencies, however, both the experiments and the microscopic analysis give $\alpha \propto \omega$. This discrepancy is not surprising, considering that the continuum theory should fail at small length scales (see above).

C. Generalization of the Griffith criterion

The Griffith criterion is a fundamental element in the theory of fracture²⁷. According to Griffith, a crack starts to advance if, in increasing its length by δL , the elastic energy released is greater than the amount of energy needed to create the new fracture surface. Mott was the first to include kinetic effects in Griffith's analysis^{27,28}. He proposed to add a kinetic energy to the Griffith's total energy. However some of the conclusions inferred from Mott's analysis are not valid, for instance the predicted value for the maximum crack speed was lower than expected (see¹ for a full discussion).

Here use a different approach and attempt to directly generalize the Griffith criterion to the viscous case by keeping track of the energy flows. We balance the energy release, the difference of the elastic energy and the surface energy, with losses due to viscous dissipation. We consider a long system of width W and thickness d , with a crack of length L . To estimate the elastic energy release E_r , we note that for $L \ll W$ a roughly round region of diameter L is fully relaxed, so that $E_r \propto \epsilon^2 L^2 d$ where ϵ is the strain that causes the material to break. For $L \gg W$ we must put $E_r \sim \epsilon^2 W L d$. The second term, the cost of creating new fracture surface E_f , is $E_f \propto L d$. Finally, the dependence of the rate of viscous dissipation δE_d on the crack speed v , may be estimated for slow cracks from a symmetry argument: Since $\delta E_d \rightarrow 0$ as $v \rightarrow 0$, and must be non-negative for any v , we conclude that $\delta E_d \propto v^2 \delta t$. The coefficient of this term goes to zero as $\eta \rightarrow 0$, so that we put $E_d \propto \eta v^2 \delta t$. Now we set $\delta E_d = \delta E_r - \delta E_f$, and use $\delta L = v \delta t$. For short cracks we see that

$$\eta v \propto \epsilon^2 L - q \quad (6)$$

where q is a constant. Short cracks accelerate. For long cracks, on the other hand, there is a *terminal velocity*:

$$\eta v \propto \epsilon^2 W - q. \quad (7)$$

If the terminal velocity is less than c_Y , the Yoffe threshold, we may expect that the crack will never branch.

Note that the analysis of this section can be expected to be valid only in the limit of low crack speed. In particular, the viscous dissipation term on the right hand side of Eq. 7 involves the motion of the lattice in response to a passing crack. Thus the η in this equation is not quite the same as the one above, and for substantial v probably has a complicated dependence on the microscopic η and on v itself. We will test these ideas with simulations, below, and find that for speeds $\ll c_R$ Eq. 7 is rather well obeyed, but that there are deviations at large speed.

D. The branching instability

The assumption in the previous section is that the critical speed for branching is independent of η , which is

what we find numerically for small η (see below). This is a bit unexpected since, in the presence of dissipation the analytical solution of Yoffe, for example,⁹ is no longer correct. We can see where this assumption would break down by examining the form of that solution.

The stress field described can be derived from an appropriate distribution of forces applied at the crack edges which have the general form $\mathbf{f}(\mathbf{r} - \mathbf{v}t)$. The stresses at an arbitrary point of the plane can be obtained by means of the Green function, $G_{ij}(\mathbf{r} - \mathbf{r}', t - t')$, with Fourier transform $G_{ij}(\mathbf{k}, \omega)$. In the absence of dissipation, the frequency ω appears only in combinations of the type $\omega^2 - c_{L,T}^2 k^2$, where $c_{L,T}$ denote the velocity of longitudinal and transverse sound waves. Dissipation changes these expressions into $\omega^2 - c_{L,T}^2 k^2 - i\eta\omega k^2/\rho$. The Fourier transform of the applied forces can be written as $\mathbf{f}(\mathbf{k}, \omega = \mathbf{v} \cdot \mathbf{k})$. Hence, the denominators in the Green's functions become $(\mathbf{v} \cdot \mathbf{k})^2 - c_{L,T}^2 k^2 - i\eta k^2 \mathbf{v} \cdot \mathbf{k}/\rho$. At low values of k , the influence of the viscosity is negligible. The long distance behavior is well described by the Yoffe solution. For large k on the other hand, the viscous term dominates. This term is more anisotropic than the inertial term, as it contains one power of $\mathbf{v} \cdot \mathbf{k}$, instead of two. Hence, we expect the tendency towards instability to be reduced. We can see when this is relevant by putting $k \sim 1/a$, and noting that large k means that $k \gg \rho v/\eta$, or equivalently, $\alpha a \gg 1$. For very large η the branching threshold should eventually shift. As we will see, we have confirmed this shift using the simulations.

V. NUMERICAL SIMULATIONS

A. Discretization of the Equations of Motion

In our simulations we work in two dimensions, and discretize the continuum equations of elasticity by using a spring model on a triangular two dimensional grid, following our previous work on quasistatic fracture²⁹⁻³¹ The equation of motion for the displacement, $\mathbf{u}_{\mathbf{r}}$ of the node at \mathbf{r} combines inertial and viscous terms. In our discrete model, we get the k^2 dependence of the attenuation by using the fact that the friction forces can depend only on the relative velocities of neighboring nodes⁸. The equations of motion are:

$$m \frac{\partial^2 \mathbf{u}_{\mathbf{r}}}{\partial t^2} = \sum_{\mathbf{r}'} K \hat{\mathbf{n}} [\hat{\mathbf{n}} \cdot (\mathbf{u}_{\mathbf{r}} - \mathbf{u}_{\mathbf{r}'})] + \sum_{\mathbf{r}'} \eta_o \hat{\mathbf{n}} \left[\hat{\mathbf{n}} \cdot \left(\frac{\partial \mathbf{u}_{\mathbf{r}}}{\partial t} - \frac{\partial \mathbf{u}_{\mathbf{r}'}}{\partial t} \right) \right] \quad (8)$$

where the sums in the second term are over the nearest neighbor nodes, \mathbf{r}' , to node \mathbf{r} and $\hat{\mathbf{n}}$ is the unit vector from node \mathbf{r}' , to node \mathbf{r} . The fracture process is described by deleting the forces between two nearest neighbor nodes when the relative strain, $|\hat{\mathbf{n}} \cdot [\mathbf{u}_{\mathbf{r}} - \mathbf{u}_{\mathbf{r}'}]|$, exceeds a threshold, u_{th} . This process is irreversible, and

the coupling remains zero at all latter times. The model used here is deterministic, and the system is always out of equilibrium.

B. The elastic constants of the model

In order to find the relationship between the parameters of our model and the experimental constants we need to write down the equation of motion of our model (Eq. (8)) in the continuum limit,

$$m \partial_{tt} \mathbf{u} = K a^2 \left[\frac{3}{8} \nabla^2 \mathbf{u} + \frac{3}{4} \nabla (\nabla \cdot \mathbf{u}) \right] + \eta_o a^2 \left[\frac{3}{8} \nabla^2 \partial_t \mathbf{u} + \frac{3}{4} \nabla (\nabla \cdot \partial_t \mathbf{u}) \right], \quad (9)$$

where a is the lattice spacing. Solving the above equations in a finite difference scheme gives Eq. (8). Then, comparing Eqs. (1) and (9) one can obtain the relations we are seeking for. First note that our model gives the following relations between the continuum parameters, $\lambda = \mu = 3E/8$ and $\psi = \eta$ and a Poisson coefficient of $1/3$. On the other hand,

$$\frac{3K}{8m} a^2 = \frac{3E}{8\rho} \quad (10)$$

where a is the lattice constant of our triangular spring network. The longitudinal and transverse sound velocities are,

$$c_L = \sqrt{3} c_T = \sqrt{\frac{\lambda + 2\mu}{\rho}} = \sqrt{\frac{9K}{8m}} a \quad (11)$$

From these results the Rayleigh speed can be easily derived⁸,

$$c_R = 0.9325 c_T \quad (12)$$

Finally, the equations which relate the constants of our model with the macroscopic parameters of the material are:

$$m = 3\rho a^2 d/8 \quad (13a)$$

$$K = 8c_T^2 m/3a^2 \quad (13b)$$

$$\eta_o = \eta d \quad (13c)$$

where d is the thickness of the sample. In the next subsection, we discuss some difficulties in relating u_{th} to macroscopic variables, particularly due to the discretization scale a .

C. Fracture threshold and macroscopic variables

In the following we take $u_{th} = 0.1a$. The process of failure is described in macroscopic terms by the maximum load above which the material fails. In our model, the maximum force exerted by the springs, Ku_{th} , should be equal to this load times the lattice spacing, a , times the thickness of the slab, d . As K is independent of a , we find that $u_{th} \propto a$.

The description of fracture by discrete element methods always leads to failure at the smallest scale. In our case, a sample under load will eventually fail through the snapping of a single row of springs, and crack widths are always of order a ³². The energy required to create a crack is, because of this effect, dependent on the discretization, and goes to zero as the lattice spacing is decreased. In the present case, the energy needed to create a crack of (macroscopic) length l goes as $\frac{l}{a}Ku_{th}^2 \propto a$. Thus, we cannot fit the tensile strength and the fracture energy at the same time in a discretization independent way. This drawback can be inferred from the existence of a characteristic length which combines these quantities, as analyzed in the introduction.

Macroscopic crack energies can be obtained from models which incorporate non local effects³³. However, detailed microscopic simulations³⁴ show cracks of atomic width, with little or no damage outside a zone of microscopic dimensions. They are also difficult to reconcile with the existence of crack energies with macroscopic values. The origin of macroscopic failure zones in quasibrittle materials such as PMMA is not well understood.

D. The dissipation term

Qualitatively, each node represents a region in the material comparable to the scales relevant to the experimental situation. In our case, we have $l_{ch} \approx 60$ microns. We use a phenomenological damping term, $\eta_o \sim 1$ in units where $K = m = 1$, which implies that sound waves at this length scale are in the overdamped regime. As mentioned earlier, the sound attenuation in glassy polymers has a complicated dependency on frequency. Our choice of η overestimates the experimental value in the GHz range²², although probably underestimates it at lower frequencies (note that our model assumes that $\alpha\Lambda \sim \Lambda^{-1}$ at all wavelengths). The scheme used here is intermediate between a full scale atomic simulation³⁴, and more phenomenological models³⁵, where dissipation takes place within the units used in the discretization.

E. Drawbacks of the model

As mentioned earlier, the main difficulty with the model is the fact that the crack energy does not scale with

the level of discretization. Only for a given lattice constant, a , the crack energy and the maximum load can be consistent with macroscopically determined values. On the other hand, instability criteria based on energy considerations, such as the Griffith criterion and extensions thereof, depend only on energy differences. Hence, we do not think that the problem discussed here is a serious obstacle to the analysis of the instabilities of moving cracks. As there are substantial differences between discrete and continuum models³⁶, it would be interesting to analyze further the relevance of the intrinsic length scale determined by the macroscopic parameters which describe fracture.

F. Numerical Procedures

Simulations have been performed in rectangular strips with the y orientation along one of the axis of the triangular lattice. The lattices shown in the figures are 50 nodes wide and 275 nodes long. The boundary condition is fixed displacement of the edges so that the initial strain is below u_{th} . Then, bonds near the lower horizontal edge are broken at a fixed rate, so that the velocity of the crack is well below c_T . To integrate the equations of motion we use Heun's method with a time step small enough for appreciate small variations in the velocity of the crack. Once the crack is sufficiently long, strains near its tip begin to exceed u_{th} , and the crack continues growing by itself. Very short cracks do not grow on their own, because the strains at the tip do not exceed u_{th} . The minimum size for self-sustained growth decreases with increasing dissipation.

VI. RESULTS

A. Stable and unstable cracks

In the absence of damping, straight cracks become unstable on short time scales. Typical results for cracks growing in a narrow slab under an applied strain at the edges are shown in Fig. 2 (a)-(c). The crack tips accelerate, exactly as predicted in Eq. (6) until they approach c_Y , and then they branch. The velocity of the uppermost part of the crack pattern is depicted in Fig. 2 (d)-(f). We note that the crack velocity strongly oscillates as a function of the crack length.

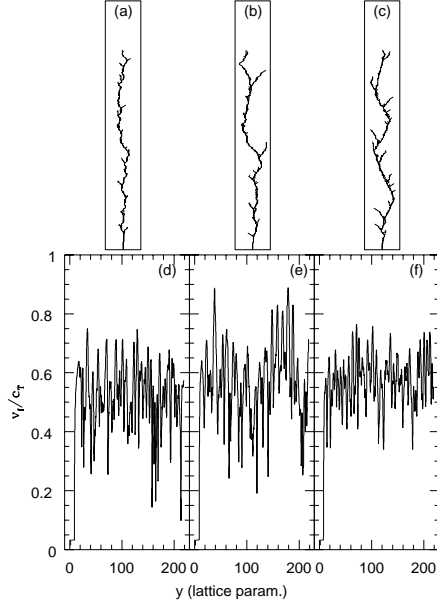


FIG. 2. Behavior of inertial cracks when the external strain, u_{appl} , is varied. (a) $u_{appl}=0.024$. (b) $u_{appl}=0.026$. (c) $u_{appl}=0.028$. And also their velocity (in units of c_T) as function of position of the advancing crack tip. (d) $u_{appl}=0.024$. (e) $u_{appl}=0.026$. (f) $u_{appl}=0.028$. The threshold for breaking is $u_{th} = 0.1$.

We find that straight cracks can be stable (cf Fig. 5a, below), and move at constant velocity, in the presence of dissipation. As the driving force is increased, we observe a branching instability. This behavior is what is predicted by Eq. (7). If the terminal velocity is below c_Y (which we assume to be independent of η , see below) the crack will be slowed down and prevented from branching. This behavior is shown in Fig. 3 where the terminal stable velocity in units of c_R is plotted against the displacement at the borders of the system. The evolution to increasing velocity proceeds as the external displacement is increased. The curves end at the branching instability. From them, we can deduce that this threshold is independent of the parameters of the simulation (size and viscosity) and $\approx 0.7c_R$, in agreement with Yoffe⁹ calculations.

The reason for the insensitivity of the branching threshold to η was given above. We find in our simulations that to shift the threshold significantly below $0.7c_R$, η must be greater than 7 for a 50×300 mesh, which is, we think, an unphysically large value. Nevertheless, the branching threshold reported in⁴ $\approx 0.45c_R$, is around 35% smaller than in the numerical simulations.

The fact that we do not see an abrupt change in the velocity before the branching threshold is related with the method we use to perform the simulations. Boudet and Ciliberto¹⁶ demonstrated experimentally that this jump was not present when sound was added into the system. This is what we do in the simulations: the slow cutting of bonds that initiate the fast failure is a source of sound

into the system.

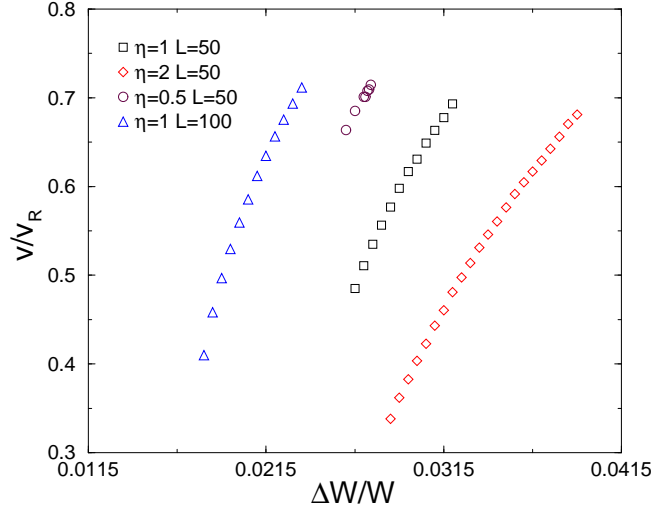


FIG. 3. Terminal velocity for a stable crack in units of the Rayleigh speed as function of the applied strain for different values of the viscosity and width of the system.

We can directly verify the validity of Eq. (7) by considering a number of different sets of the parameters ϵ , η , W , such as those shown in Fig. 3 and viewing our data in the form of a data collapse. This is done in Fig. 4 where we show that ηv is very accurately a linear function of $\epsilon^2 W$ for low speeds. For larger speeds, of the order of c_Y there are deviations from Eq. 7, as we expect.

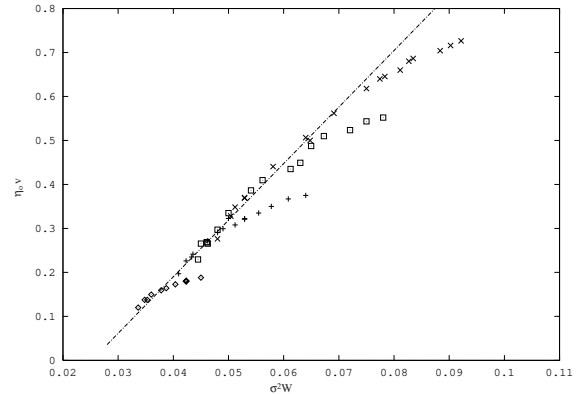


FIG. 4. Data collapse of $\eta_0 v$ plotted against $\epsilon^2 W$. $\diamond, \eta_0 = 0.5$; $+$, $\eta_0 = 1.0$; \square , $\eta_0 = 1.5$; \times , $\eta_0 = 2.0$, for $12 < W < 50$ and $0.029 < \epsilon < 0.058$. The straight line is fitted to all the points for which $v < 0.3$.

B. Thermal noise and the branching threshold

Numerically is possible to obtain lower critical branching velocities by adding a random noise in Eq. 9, as will be discussed in detail in a forthcoming publication³⁷. This

random noise is in the form that it has zero mean at its correlation is

$$\langle \gamma_i \cdot \gamma_j \rangle = \xi T, \quad (14)$$

when $i = j$, and zero otherwise. T is the temperature, and ξ is a parameter that controls numerically the amplitude of the noise. In Ref. ³⁷ ξ is related to η using the fluctuation-dissipation theorem. Here we take a more phenomenological approach in order to simply illustrate the effect.

Let us take one of the stable cracks whose velocity is plotted in Fig 3. The one with $\Delta W/W=0.03$, $\eta=1$, and $L=50$ has a velocity of $\approx 0.65c_R$. Fig. 5 show the shape of the cracks for different values of ξ . The temperature is set to a fixed arbitrary value of 100. When the noise is very low (10^{-9}) nothing happens to the crack. When it becomes higher, always at the same terminal velocity, small side branches like in the experiments can be obtained. The spacing between branches decreases as the noise intensity is increased, and, in some cases (see Fig. 5(c)), the crack can destabilize at later stages in the growth process, until finally the crack becomes unstable (Fig. 5(d)).

Since in our simulations we have all the information of the displacements at all points of the network, we can compute the stress tensor at any time of the evolution of the crack. In particular it is interesting to see the values of $\sigma_{yy} - \sigma_{xx}$ around the crack tip. According to Cotterell and Rice³⁹, this quantity describes the stability of the cracks. It should be less than zero at the crack tip for an stable crack and greater than zero when it becomes unstable. This parameter is shown in the lower part of Fig. 5 when the corresponding cracks in the upper part of the figure have advanced half the length of the system. The three cracks with lower noise intensity are, according to this criterion, still stable, but the one with higher noise has a tendency to continue deviating to the left.

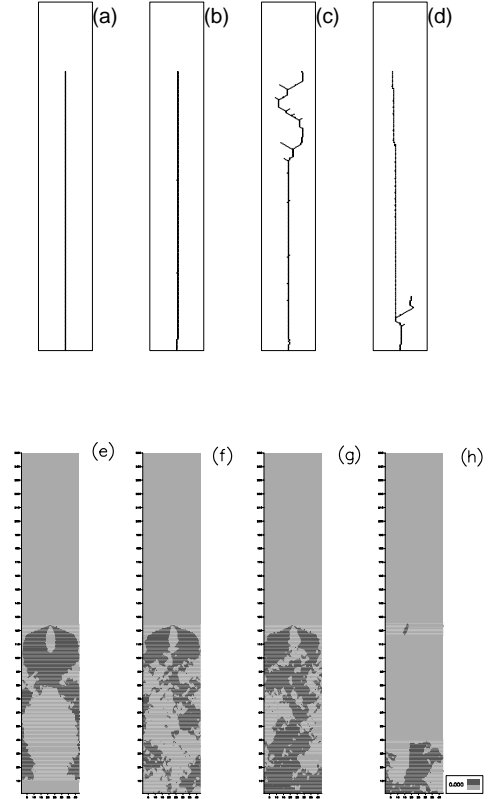


FIG. 5. Shapes of the cracks when noise is added (a) $\xi = 10^{-9}$, (b) $\xi = 4 \times 10^{-8}$, (c) $\xi = 10^{-7}$, and (d) $\xi = 2 \times 10^{-7}$. The lower figures (e-h) show the sign of the Cotterell and Rice parameter ($\sigma_{yy} - \sigma_{xx}$): dark grey positive and light grey negative. Stresses are taken when the crack has advanced half the length of the system. The noise is the one of the corresponding above figure (a-d).

This method for representing the stress tensor with a wide variety of parameters in an elastic medium can provide a valuable tool for inspecting the conditions for the stability, and the analytical approximations that can be made⁴⁰.

VII. HEATING AND ENERGY DISSIPATION

In the previous section, examples of crack propagation in the presence of thermal noise due to an external environment, have been discussed. However, the local temperature around the crack tip must also take into account the energy dissipated by the viscosity term that we have in the equations. Near the crack tip typical deviations of the nodes from equilibrium are of order a . Typical velocities are of order Ku_{th}/η_0 . The energy dissipated per node and per unit time is $\sim K^2 u_{th}^2 / \eta_0$. In terms of macroscopic quantities, the energy generated per unit time and unit volume is $\sim \rho^2 c^4 a^2 \sigma_c^2 / (\mu E^2)$, where c is some average of the longitudinal and transverse sound ve-

locities, E is the Young's modulus and σ_c is the macroscopic elastic limit. This dissipation generates thermal gradients. They will be determined by the condition:

$$\frac{\partial T}{\partial t} = \kappa \nabla^2 T + \frac{1}{\rho c_e} \frac{\partial \mathcal{E}}{\partial t} = 0 \quad (15)$$

where κ is the thermal diffusion coefficient, \mathcal{E} is the energy being dissipated and c_e is the specific heat. Assuming that most of the dissipation takes place at distances from the crack tip comparable to its radius, we find that the temperature increase at the tip can be written as: $\Delta T_{tip} \sim c^4 a^4 \sigma_c^2 / (\kappa \mu c_e E^2)$. This expression is highly sensitive to the choice of a , the tip radius. Hence, it is difficult to make accurate estimates of the expected heating. Experimentally, significant increases in temperature near the crack tip have been reported¹⁵. Energy dissipation has also been observed in⁵, where it is argued that most of the energy is spent in increasing the crack surface. However, even for slow, straight cracks, a significant rise in energy dissipation as function of velocity is reported. In our simulations the elastic energy lost when one spring is cut goes into surface energy, whereas the viscous dissipation goes into heat. Heating of the crack tip increases thermal noise there. This could be quite significant since, near, but below the branching speed the stress distribution becomes nearly isotropic, so that relatively small thermal effects could lead to branching. The considerations in this section will be worked out in detail in Ref.³⁷.

VIII. CONCLUSIONS

The analysis reported here indicates that viscous effects change significantly the propagation, and instabilities, of cracks in brittle materials. The general features that we have found should be reproduced, for example, in PMMA, even though the viscosity is a more complicated function of frequency than the one considered here. Some of the characteristics of the experimental results^{2,3,5,4} are already qualitatively described by the present approach. In particular, our approach would explain why experiments in glass are harder to perform than in PMMA: its associated viscosities are lower than in PMMA and thus it is closer to the instability. On the other hand, the branching threshold seems to be lower in the experiments than in our numerical simulations for the chosen parameters. This fact has also been discussed and shown to be due to other effects not contained within the model, but that can be incorporated as external noise. Of course, the richness and complexity of fracture in these materials will require further investigations. We hope that the approach herewith proposed will help to improve our understanding of these interesting phenomena.

IX. ACKNOWLEDGMENTS.

We acknowledge many fruitful discussions with J. Planas, J. Colmenero, F. Abrahams, P. Español and M. A. Rubio. We are also grateful to S. Ciliberto and J.-F. Boudet for a most illuminating description of the experimental situation. FG is supported by CICYT grant no. PB96-0875, EL by CICYT grant no. PB96-0085, and LMS and SVG by NSF grant DMR 94-20335. LMS also acknowledges help from the Iberdrola Foundation.

X. APPENDIX

The energy dissipated by sound waves goes into other excitations of the system. Taking the sound velocity of PMMA to be $v_s \approx 10^5$ cm/s, a mode of wavelength of one micron has a frequency of 10^9 Hz. In energy units, it corresponds to $\approx 7 \times 10^{-7}$ eV. At sufficiently low temperatures, the main source of inelastic scattering at these frequencies, as seen by neutron scattering, is quantum tunneling between equivalent configurations of the CH₃ groups attached to the polymer²⁶. The possibility that these excitations play a role in sound attenuation was suggested in²⁵.

An acoustical phonon modulates the distance between polymers. At the low frequencies involved, the backbone of the polymer cannot be excited, and can be considered rigid. The motion of a nearby polymer changes the potential acting on a given CH₃ group, breaking the initial threefold symmetry. The asymmetry in the potential induces transitions between the quantum levels of the CH₃ group, and leads to dissipation.

The interaction between the neutral CH₃ unit and other parts of the polymer arise from mutual induced polarization. Assuming that neither part has a finite electric dipole, the interaction energy is given by the van der Waals expression:

$$E = \frac{e^4}{\epsilon^2 r^6} \sum_{m,n} \frac{|\vec{d}_m^a \vec{d}_n^b - 3(\vec{d}_m^a \vec{r})(\vec{d}_n^b \vec{r})/r^2|^2}{\Delta_m + \Delta_n} \quad (16)$$

where r is the distance, ϵ is the dielectric constant due to the rest of the material, $\vec{d}_m^a = \langle 0 | \vec{r} | m \rangle$ represents a matrix element of \vec{r} between states of unit a (and a corresponding expression for \vec{d}_n^b), and Δ_m is the energy difference between the ground state of unit a and a given excited state.

The order of magnitude of E in (16) is $E \sim \frac{e^4 d^4}{\epsilon^2 r^6 \Delta}$, where d goes as the dimension of the unit, Δ is a typical electronic excitation energy, and r is the separation.

The splitting between configurations of the CH₃ unit goes as the difference in the interaction energy (16) at nearby H sites. Hence, it goes as $\frac{\partial E}{\partial r} d_{H-H}$.

A phonon which induces displacements \vec{u}_k in a given molecule leads to a change in the intermolecule distance

r of order $(\vec{k}\vec{r})\vec{u}_k$. Using the golden rule, the energy per unit time absorbed by a given CH₃ group goes as:

$$\frac{\partial E}{\partial t} = \frac{1}{\hbar} \left(\frac{e^4 d^4}{\epsilon^2 r^6 \Delta} \right)^2 \frac{d_{H-H}^2}{r^2} k^2 u_k^2 \omega_{ph} \rho_{tunn}(\omega_{ph}) \quad (17)$$

where $\rho_{tunn}(\omega)$ is the density of tunneling centers of energy splitting ω . The energy dissipated per unit volume can be estimated from (17) by multiplying that expression by the number of CH₃ groups per molecule, N , and dividing by the volume of the molecule, Ω .

On the other hand, the energy dissipated per unit volume, can be written as⁸:

$$\frac{\partial E}{\partial t} \propto \eta \omega_{ph}^2 k^2 u_k^2 \quad (18)$$

where η stands for an average of the macroscopic viscosity. In terms of η , the sound attenuation goes as $\frac{\eta \omega_{ph}^2}{\rho c^3}$, where ρ is the density, and c is the sound velocity. Making use of the microscopic parameters, this gives:

$$\alpha \sim k \frac{N}{\hbar \rho \Omega c^2} \frac{d_{H-H}^2}{r^2} \left(\frac{e^4 d^4}{\epsilon^2 r^6 \Delta} \right)^2 \rho_{tunn}(\omega_{ph}) \quad (19)$$

This expression is very sensitive to the value of r , the distance between nearby chains. A rough estimate can be made by assuming $\frac{\rho \Omega c^2}{N} \sim \Delta \sim 1\text{eV}$, $d_{H-H} \sim d \sim 1\text{\AA}$, $r \sim 5\text{\AA}$, $\rho(\omega) \sim (1\mu\text{eV})^{-1}$ and $\epsilon = 1$. Using these parameters, we obtain $\alpha \Lambda \sim 1-10$, where Λ is the wavelength of the phonon. The dependence on frequency of $\alpha \Lambda$ is that of $\rho_{tunn}(\omega)$, which, in the relevant range of frequencies, $\sim 1\mu\text{eV}$, is roughly constant²⁶. This gives $\alpha \propto \omega$, in line with²². Below lower frequencies, $\sim 1\text{kHz}$, $\rho_{tunn}(\omega) \propto \omega$, leading to $\alpha \Lambda \propto \Lambda^{-1}$, and $\alpha \propto \omega^2$, similar to the behavior reported in²³.

Quantum tunneling is suppressed by thermal fluctuations, which break the degeneracy of the three potential minima seen by the CH₃ groups. We assume that these fluctuations arise from changes in the van der Waals interactions with neighboring polymers. The presence of a lattice vibration, of momentum k and amplitude u_k induces a splitting between equivalent minima of:

$$\Delta E \sim \frac{e^4 d^4}{\epsilon^2 r^6 \Delta} \frac{d_{H-H}}{r} k u_k \quad (20)$$

The derivation of this expression follows the analysis presented earlier. At finite temperatures, u_k shows random fluctuations. The mean square deviation of ΔE is given by:

$$\langle (\Delta E)^2 \rangle \sim \left(\frac{e^4 d^4}{\epsilon^2 r^6 \Delta} \right)^2 \frac{d_{H-H}^2}{r^2} \langle k^2 u_k^2 \rangle \quad (21)$$

and:

$$\langle k^2 u_k^2 \rangle \sim \Omega \int^{\hbar c k \ll k_B T} d^3 k \frac{k^2 k_B T}{\rho \Omega \hbar^2 c^2 k^2} \sim \frac{k_B T}{\Omega \rho c^2} \left(\frac{T}{\omega_D} \right)^3 \quad (22)$$

where ω_D is the Debye temperature. In terms of the attenuation rate calculated above, we can write:

$$\langle (\Delta E)^2 \rangle \sim \frac{\alpha \Lambda}{N} \frac{k_B T}{\rho_{tunn}(E)} \left(\frac{T}{\omega_D} \right)^3 \quad (23)$$

Using the same parameters as above, and setting $\omega_D = 300\text{K}$, we find that the fluctuations ΔE are of order $1\mu\text{eV}$ when $T \sim 10\text{K}$.

At higher temperatures, the dynamics of CH₃ groups lose coherence. They still influence sound attenuation, because they mediate interactions between phonons.

Note, finally, that the mechanism discussed here does not lead to plastic effects. The material remains brittle at the scales of interest, as it seems to be the case in PMMA. Other mechanisms, such as the irreversible relaxation of structural defects, may lead to viscoplastic effects³⁸.

¹ L. B. Freund, *Dynamic Fracture Mechanics* (Cambridge University Press, New York, 1990).

² J. Fineberg, S. P. Gross, M. Marder, and H. L. Swinney Phys. Rev. B **45**, 5146 (1992).

³ J.F. Boudet, S. Ciliberto, and V. Steinberg, Europhys. Lett. **30**, 337 (1995).

⁴ J. F. Boudet, S. Ciliberto and V. Steinberg, J. Phys. II **6**, 1493 (1996).

⁵ E. Sharon, J. Fineberg and S. P. Gross, Phys. Rev. Lett. **74**, 5096 (1995).

⁶ E. Sharon, S.P. Gross, and J. Fineberg, Phys. Rev. Lett. **76**, 2117 (1996).

⁷ A. Yuse and M. Sano, Nature **362**, 329 (1993).

⁸ L. Landau and E. Lifshitz, *Theory of Elasticity*, Addison-Wesley, 1959.

⁹ E. H. Yoffe, Phil. Mag. **42**, 739 (1951).

¹⁰ M. Adda-Bedia and M. Ben Amar, Phys. Rev. Lett. **76**, 1497 (1996).

¹¹ M. Adda-Bedia, R. Arias, M. Ben-Amar and F. Lund, preprint (1998).

¹² J. Gálvez, M. Elices, G. V. Guinea and J. Planas, Int. Journ. of Fracture **81**, 171 (1996).

¹³ F. J. Gómez Sánchez, Ph. D. thesis. Universidad Politécnica de Madrid (1998).

¹⁴ O. Pla, Modelling Simul. Mat. Sci. Eng. **4**, 193 (1996).

¹⁵ K. N. G. Fuller, P. G. Fox and J. E. Field, Proc. R. Soc. Lond. A **341**, 537 (1975).

¹⁶ J. F. Boudet and S. Ciliberto, Phys. Rev. Lett. **80**, 341 (1998).

¹⁷ S. P. Gross, J. Fineberg, M. Marder, W. D. McCormick and H. L. Swinney, Phys. Rev. Lett. **71**, 3162 (1993).

¹⁸ J. F. Boudet, private communication.

¹⁹ J. S. Langer, Phys. Rev. Lett. **70**, 3592 (1993).

²⁰ J. J. Freeman and A. C. Anderson, Phys. Rev. B **34**, 5685 (1986).

²¹ D. A. Jackson, H. T. A. Pentecost and J. G. Powles, Molec. Phys. **23**, 425 (1972).

- ²² C. J. Morath and H. J. Maris, Phys. Rev. B **54**, 203 (1996).
- ²³ B. Hartmann in *Physical Properties of Polymers Handbook*, J. E. Mark ed., AIP Press (New York, 1996).
- ²⁴ I. Perepeckhko, *Low temperature properties of polymers*, Pergamon (Oxford, 1980).
- ²⁵ J. Williams and A. Eisenberg, Macromolecules **11**, 700 (1978).
- ²⁶ J. Colmenero, R. Mukhopadhyay, A. Alegría and B. Frick, Phys. Rev. Lett., **80**, 2350 (1998).
- ²⁷ A. A. Griffith, Phil. Trans. R. Soc. (London) **A221**, 163 (1920).
- ²⁸ N.F. Mott, Engineering **165**, 16 (1948).
- ²⁹ E. Louis and F. Guinea, Europhys. Lett. **3**, 871 (1987).
- ³⁰ P. Meakin, G. Li, L.M. Sander, E. Louis, and F. Guinea, J. Phys. A **22**, 1393 (1989).
- ³¹ O. Pla, F. Guinea, E. Louis, G. Li, L. M. Sander, H. Yan, and P. Meakin, Phys. Rev. A **42**, 3670 (1990).
- ³² Z. P. Bazant and J. Planas, *Fracture and Size Effect in Concrete and Other Quasibrittle Materials*, CRC Press (New York), 1998.
- ³³ J. Planas, M. Elices and G. V. Guinea in *Fracture and Damage in Quasibrittle Structures*, Z. P. Bazant, Z. Bittnar, M. Jirasek and J. Mazars eds. E & FN Spon (London), 1994.
- ³⁴ F. F. Abraham, Phys. Rev. Lett. **77**, 869 (1996).
- ³⁵ M. Marder and S.P. Gross, J. Mech. Phys. Solids **43**, 1 (1995).
- ³⁶ D. A. Kessler and H. Levine, *Steady-State Cracks in Viscoelastic Lattice Models*, preprint (cond-mat/9812164).
- ³⁷ L. Sander and S. Ghaisas, preprint.
- ³⁸ M. L. Falk and J. S. Langer, Phys. Rev. E **57**, 7192 (1998).
- ³⁹ B. Cotterell and J.R. Rice, Int. J. Fract. **16**, 155 (1980).
- ⁴⁰ F. Guinea, O. Pla, and E. Louis, in preparation.